Sensitivity to Horizontal Resolution in the AGCM Simulations of Warm Season Diurnal Cycle of Precipitation over the United States and Northern Mexico

MYONG-IN LEE,*,+ SIEGFRIED D. SCHUBERT,+ MAX J. SUAREZ,+ ISAAC M. HELD,# ARUN KUMAR,@ THOMAS L. BELL,+ JAE-KYUNG E. SCHEMM,@ NGAR-CHEUNG LAU,# JEFFREY J. PLOSHAY,# HYUN-KYUNG KIM,@ AND SOO-HYUN YOO@,&

* *Goddard Earth Sciences and Technology Center, University of Maryland, Baltimore County, Baltimore, Maryland*
+ *NASA Goddard Space Flight Center, Greenbelt, Maryland*
# *NOAA/Geophysical Fluid Dynamics Laboratory, Princeton, New Jersey*
@ *NCEP/Climate Prediction Center, Camp Springs, Maryland*
& *RS Information Systems, Inc., McLean, Virginia*

(Manuscript received 12 December 2005, in final form 22 May 2006)

ABSTRACT

This study examines the sensitivity of the North American warm season diurnal cycle of precipitation to changes in horizontal resolution in three atmospheric general circulation models, with a primary focus on how the parameterized moist processes respond to improved resolution of topography and associated local/regional circulations on the diurnal time scale. It is found that increasing resolution (from approximately 2° to ½° in latitude–longitude) has a mixed impact on the simulated diurnal cycle of precipitation. Higher resolution generally improves the initiation and downslope propagation of moist convection over the Rockies and the adjacent Great Plains. The propagating signals, however, do not extend beyond the slope region, thereby likely contributing to a dry bias in the Great Plains. Similar improvements in the propagating signals are also found in the diurnal cycle over the North American monsoon region as the models begin to resolve the Gulf of California and the surrounding steep terrain. In general, the phase of the diurnal cycle of precipitation improves with increasing resolution, though not always monotonically. Nevertheless, large errors in both the phase and amplitude of the diurnal cycle in precipitation remain even at the highest resolution considered here. These errors tend to be associated with unrealistically strong coupling of the convection to the surface heating and suggest that improved simulations of the diurnal cycle of precipitation require further improvements in the parameterizations of moist convection processes.

1. Introduction

The ability to correctly simulate the diurnal cycle of warm season precipitation is an important test for global climate models. Studies of the diurnal cycle in carefully controlled model experiments can serve to validate the physical parameterizations (e.g., Slingo et al., 1987; Garratt et al. 1993; Chen et al. 1996; Dai et al. 1999; Dai and Trenberth 2004; Liang et al. 2004; Dai 2006), enhance our understanding of the important mechanisms that drive the diurnal cycle (e.g., Randall et al. 1991), and provide guidance on how to improve the representation of subgrid-scale processes in the model (e.g., Betts et al. 1996; Giorgi and Shields 1999; Lin et al. 2000; Groisman et al. 2000; Yang and Slingo 2001; Zhang 2003; Collier and Bowman 2004; Lee et al. 2007).

Although current climate models simulate reasonably well the broad-scale characteristics of the diurnal cycle of warm season precipitation, there are still many features at the local/regional scales that are poorly represented or unresolved (Dai and Trenberth 2004; Collier and Bowman 2004; Dai 2006). Simulating the diurnal cycle in the vicinity of the complex terrain (such as the downstream side of the Rocky Mountains, the Sierra Madre Occidental, the Tibetan Plateau, and the Amazonian basin) is extremely challenging, and many models fail to capture the nocturnal development of convection in those regions. This is likely the result of inadequate representation of the surface boundary forcing (i.e., orography and land–sea contrast) in global climate models that are typically run at a horizontal resolution of several hundred kilometers, as well as

Corresponding author address: Dr. Myong-In Lee, Global Modeling and Assimilation Office, NASA Goddard Space Flight Center, Code 610.1, Greenbelt, MD 20771.
E-mail: milee@gmao.gsfc.nasa.gov

DOI: 10.1175/JCLI4090.1

limitations in the parameterization of moist convection (Dai et al. 1999; Zhang 2003; Liang et al. 2004; Lee et al. 2007).

While the diurnal cycle of atmospheric convection over the continents is largely controlled by the direct thermodynamic response to insolation and surface heating, there are nevertheless large geographical variations in the response that are the result of a number of different forcing mechanisms. These mechanisms can be classified into three categories, according to their horizontal scale: 1) local convective instability induced by boundary heating (Machado et al. 2002); 2) regional controls from differential heating such as land–sea circulations, topography, surface vegetation type (Machado et al. 2004), and mesoscale convective systems (Maddox 1980; Riley et al. 1987; Arritt and Mitchell 1994; Carbone et al. 2002); and 3) large-scale or subcontinental controls such as the nocturnal low-level jet (Rasmusson 1967; Helfand and Schubert 1995; Higgins et al. 1997; Schubert et al. 1998), atmospheric tides (Dai and Deser 1999; Dai et al. 1999; Lim and Suh 2000), thermally driven large-scale land–ocean circulation and regional subsidence (Silva Dias et al. 1987; Figueroa et al. 1995; Gandu and Silva Dias 1998; Dai and Deser 1999; Dai 2001), and the seasonal march of the summer monsoon and basic-state changes (Machado et al. 2004). All these forcing mechanisms can potentially contribute to a complicated and localized response in the diurnal cycle of precipitation.

The purpose of this study is to evaluate the impact of increased horizontal resolution on the simulation of the warm season diurnal cycle of precipitation over the continental United States and Mexico, with a special focus on the Great Plains and the North American Monsoon Experiment (NAME; Higgins et al. 2006) regions. Specifically, we examine the impact of resolution changes on the diurnal cycle of precipitation in three different atmospheric general circulation models (AGCMs): namely the National Centers for Environmental Prediction (NCEP) model, the Geophysical Fluid Dynamics Laboratory (GFDL) model, and the National Aeronautics and Space Administration/Global Modeling and Assimilation Office (NASA/GMAO) model. This is a companion study to Lee et al. (2007), who investigated the diurnal cycle of warm season rainfall over North America in the same models but at a relatively coarse resolution (about 2°, referred to here as the standard resolution) typical of climate model simulations. The major findings of that study are that, although the overall patterns of time-mean (summer) rainfall and low-level winds are reasonably well simulated, there are substantial regional deficiencies in simulating the diurnal cycle of precipitation. Especially prominent among them are the discrepancies in the diurnal cycle of precipitation over the eastern slopes of the Rocky Mountains and the adjacent Great Plains, including the failure to adequately capture the observed nocturnal peak. Moreover, the observed late afternoon–early evening eastward propagation of convection from the mountains into the Great Plains is not properly simulated, and this contributes to the overall dry bias and other deficiencies in the diurnal cycle in the Great Plains. They ascribed this failure to the unresolved mesoscale convective systems that propagate eastward from the mountains, and the parameterized convection schemes that are too strongly tied to the boundary layer heating and rather insensitive to the free-atmospheric large-scale dynamical forcing, for example, the low-level jets. In other regions such as the southeastern United States and the North American monsoon region, the diurnal phase of rainfall has a maximum in local afternoon with a tendency to rain 2–5 h earlier than observed, depending on the models. The coarse-resolution models were not able to resolve important local circulation features such as those associated with the complex terrain of the North American monsoon region.

In extending the study of Lee et al. (2007), we carried out a number of May–September simulations with the same three AGCMs, but with varying horizontal resolution (from the standard resolution of about 2° up to ½° latitude–longitude). We focus on the impact of resolution on the diurnal cycle of rainfall over the Great Plains and the North American monsoon regions. The model simulations are validated with respect to surface rain gauge observations, high-resolution satellite measurements, reanalysis data, and recent NAME (Higgins et al. 2006) field observations.

Section 2 describes the models, experiments, datasets, and validation methods. Section 3 describes the impact of the resolution changes on the seasonal-mean precipitation simulations. Section 4 describes the impact of the resolution changes on the broad-scale characteristics of the simulated diurnal cycle of precipitation. Section 5 describes some of the key regional impacts, focusing on the Great Plains and the North American monsoon region. The conclusions are given in section 6.

2. Experiments and validation

a. Models and experiments

The three AGCMs examined in this study are those developed independently by NASA/GMAO [NASA Seasonal-to-Interannual Prediction Project version 2 (NSIPP-2), Bacmeister et al. (2000)], GFDL [GFDL

TABLE 1. The summary of the model characteristics and the experiments.

Model/version	Resolution: Horizontal (lat × lon)	Resolution: Vertical	No. of ensembles
NASA/GMAO	2° × 2.5°	L40	5
NSIPP-2	1° × 1.25°		5
	0.5° × 0.625°		2
GFDL AM2	2° × 2.5°	L24	5
	1° × 1.25°		5
	0.5° × 0.625°		5
NCEP GFS v2	T62 (~2° × 2°)	L64	5
	T126 (~1° × 1°)	L42	5
	T170 (~0.75° × 0.75°)	L42	5

Global Atmosphere Model (AM2); Anderson et al. (2004)], and NCEP [Global Forecasting System (GFS) version 2]. The dynamical and physical schemes of the models are described in detail in Lee et al. (2007). As in Lee et al. (2007), we again focus on simulations of the diurnal cycle carried out with prescribed climatological-mean monthly sea surface temperature (SST) forcing, which was obtained from a 20-yr (1983–2002) average of the Reynolds et al. (2002) optimum interpolation (OI) SST dataset. Table 1 summarizes the model characteristics and experiments. The experiments for each model consist of ensembles of runs at three different horizontal resolutions: standard (~2°), medium (~1°), and high (~½° in the NASA and GFDL runs and ~¾° in the NCEP runs). To increase the reliability of the statistics of the diurnal cycle, especially for the rainfall, five ensemble members were generated with each model. Each ensemble member was integrated for 5 months, beginning on 1 May with different atmospheric and land surface initial states: these states were taken from different years of preexisting long simulations forced with observed SSTs. The diurnal cycle was computed from hourly model outputs for the three summer months of June, July, and August (JJA), allowing for a 1-month spinup (September was not used in the analysis).

We prescribe a climatological-mean SST forcing in order to avoid potential statistical sampling problems associated with interannual variability. Based on the results from the NASA/GMAO model, we note that the ensemble average of the simulated diurnal cycle driven by the climatological-mean SST is not qualitatively different from the multiyear-averaged diurnal cycle obtained from a run with interannually varying SST condition. While differences in the initial soil moisture can have a substantial impact on the simulated rainfall in some regions, such as the Great Plains (Koster et al. 2004), any impacts on the diurnal cycle of rainfall tend to be confined to the amplitude (not the phase) of the diurnal cycle. The other two AGCMs exhibit similar behavior, showing little spread in the phase of the diurnal cycle among the individual ensemble members (Lee et al. 2007).

It must be pointed out that the higher-resolution NCEP runs (T126 and T170) were made with 42 vertical levels compared with 64 vertical levels for the T62 run, so that we cannot distinguish between the impacts of changes in the vertical and horizontal resolutions for those cases. Also, only two ensemble runs were conducted for the high-resolution cases in the NASA/GMAO model (compared with the usual five members), but this does not appear to impact the results substantially.

b. Validation

Several observed precipitation datasets are used to validate the simulated diurnal cycle of rainfall. These include the hourly precipitation dataset (HPD; Higgins et al. 1996) constructed by NCEP/Climate Prediction Center (CPC), and analyzed to a 2° × 2.5° latitude–longitude grid. The high temporal resolution (hourly) and long record (more than 50 yr from 1948) makes this an ideal dataset for estimating the diurnal cycle of precipitation (e.g., Dai et al. 1999). This study used the HPD dataset for the recent 20-yr period (1983–2002), which is consistent with the SST forcing period. The relatively coarse horizontal resolution of the data, however, makes it unsuitable for comparing with our high-resolution runs. The higher-resolution runs are instead validated against the 3-hourly assimilated rainfall products (30-km horizontal resolution) from the NCEP North American Regional Reanalysis (NARR; Mesinger et al. 2006). The NARR assimilates surface rain gauge observations so that the diurnal cycle of the rainfall is very similar to that of the HPD over the continental United States. We also use the 3-hourly (¼° spatial resolution) satellite-based CPC Morphing Technique rainfall product (CMORPH, Joyce et al. 2004), although it is only available for the recent 3-yr period (2003–05). For the North American monsoon domain we validate the diurnal cycle using the hourly precipitation data from the NAME Event Rain Gauge Network (NERN; Gochis et al. 2004), which is available for the period of 2003–04. The NCEP/CPC 1° × 1° daily gridded precipitation analysis over North America (Higgins et al. 2000) was used to validate the seasonal-mean rainfall based on the period 1983–2002. In addition, we used the 3-hourly NARR 925-hPa winds averaged over the same time period (1983–2002) to validate the diurnal variation of the low-level winds.

In defining the amplitude and phase of the observed and simulated diurnal cycle of precipitation, we first construct a mean 24-h diurnal time series of rainfall by averaging the precipitation amount hour by hour over the entire time period available. For example, for the NCEP HPD we have a total of 92 days by 20 summers available for averaging. This "climatological mean" diurnal cycle was then decomposed using Fourier harmonic analysis to determine the amplitude and phase of the wavenumber 1 (24-h cycle) component. We examine only the first harmonic of the 24-h cycle because it dominates over most of the land areas. We test the estimated amplitude and phase of the diurnal cycle of rainfall for statistical significance using the method described in the appendix.

3. Seasonal-mean precipitation simulations

Figure 1 compares the summer (JJA) mean precipitation from the observations and the ensemble means of the three AGCMs at the three different horizontal resolutions (standard, medium, and high). Results from two different observed products are presented in the figure; one is from the NCEP/CPC 1° × 1° daily precipitaton analysis (Fig. 1a, average of 1983–2002) and the other is from the ¼° × ¼° CMORPH (Fig. 1b, average of 2003–05). Compared with the observed precipitation pattern (Fig. 1a), the standard resolution (~2°) runs (Figs. 2c–e) have similar dry biases in the upper Great Plains–Midwest, and areas of wet bias over the Rocky Mountains. In fact, the locations of the wet biases over the Rockies show the greatest similarity in the high-resolution runs (Figs. 2i–k), suggesting an increased locking of the precipitation to the high terrain. This strong link to topography is especially evident in the NASA model (Fig. 2i), which shows signatures of the Rocky Mountains, the Sierra Madre Occidental (SMO), and the Appalachians in the precipitation climatology of the high-resolution runs. Excessive rainfall over the high terrain seems to be an artificial feature in the models. This feature is not evident in the high-resolution CMORPH observations (Fig. 1b), where the local rainfall maxima are located downstream of the elevated regions of the Rockies and the Appalachians.

A key improvement obtained with the increased resolution is in the simulation of the summertime North American monsoon. In general, the higher-resolution runs tend to confine the rainfall more to the western slope of the SMO, similar to the observed precipitation patterns (e.g., the GFDL model). They also tend to simulate increased rainfall over northern Mexico and southern Arizona–New Mexico, although the highest-resolution runs are still dry in the Arizona and New Mexico region. In other regions, the resolution impacts are somewhat mixed and no systematic changes can be found. The NCEP T126 runs (Fig. 1h) show a generally improved rainfall simulation over the Midwest, while that is not true for the T170 runs (Fig. 1k).

4. Diurnal cycle in precipitation

a. Amplitude

Figure 2 compares the amplitude (mm day^{-1}) of the diurnal cycle of hourly precipitation (the 24-h harmonic), with the ratio of the amplitude to the daily mean shown in Fig. 3. The observed values from the long-term (1983–2002) hourly precipitation records (HPD shown in Figs. 2a and 3a) exhibit large amplitude over the southern and eastern United States, where they reach values of more than 70% of the daily mean precipitation amount, which is consistent with Dai et al. (1999). The central United States also shows strong diurnal variations, particularly over the eastern side of Rocky Mountains and the adjacent plains. The estimated amplitudes from the CMORPH observations (Fig. 2b) are much larger than those in the HPD (Fig. 2a), even though they are estimated from the 3-hourly rainfall time series. This is likely due to the relatively small sample size of the CMORPH observations (three summers in 2003–05), and a possible positive bias of the satellite estimates over land (Janowiak et al. 2007). When the diurnal amplitudes are normalized by the seasonal means, the two datasets are more consistent, with both showing a coherent geographical pattern (cf. Figs. 3a and 3b).

At the standard resolution, the NASA model has too strong diurnal variations compared with the HPD observations, and the amplitude tends to increase with increasing model resolution (cf. Figs. 2c, 2f, and 2i). At all of the resolutions, the amplitude of the diurnal cycle of the rainfall in the NASA model is comparable to the seasonal-mean precipitation amount (Figs. 3c, 3f, and 3i). In some locations such as the Rocky Mountains, the diurnal amplitudes are much larger than the seasonal-mean rainfall amount. This (erroneous) feature implies that the precipitation processes that contribute to the overall time-mean wet biases over this region are strongly tied to the diurnal cycle, characterized by strong short-duration showers and dry conditions for the rest of the day. This feature will be discussed in more detail in the next section. Unlike the NASA model, the GFDL model has relatively weaker diurnal variations in the standard resolution runs, compared with the HPD, but it has the same tendency for the amplitude to increase with increasing resolution (cf. Fig. 3). The NCEP (Figs. 2e, 2h, and 2k) model has a

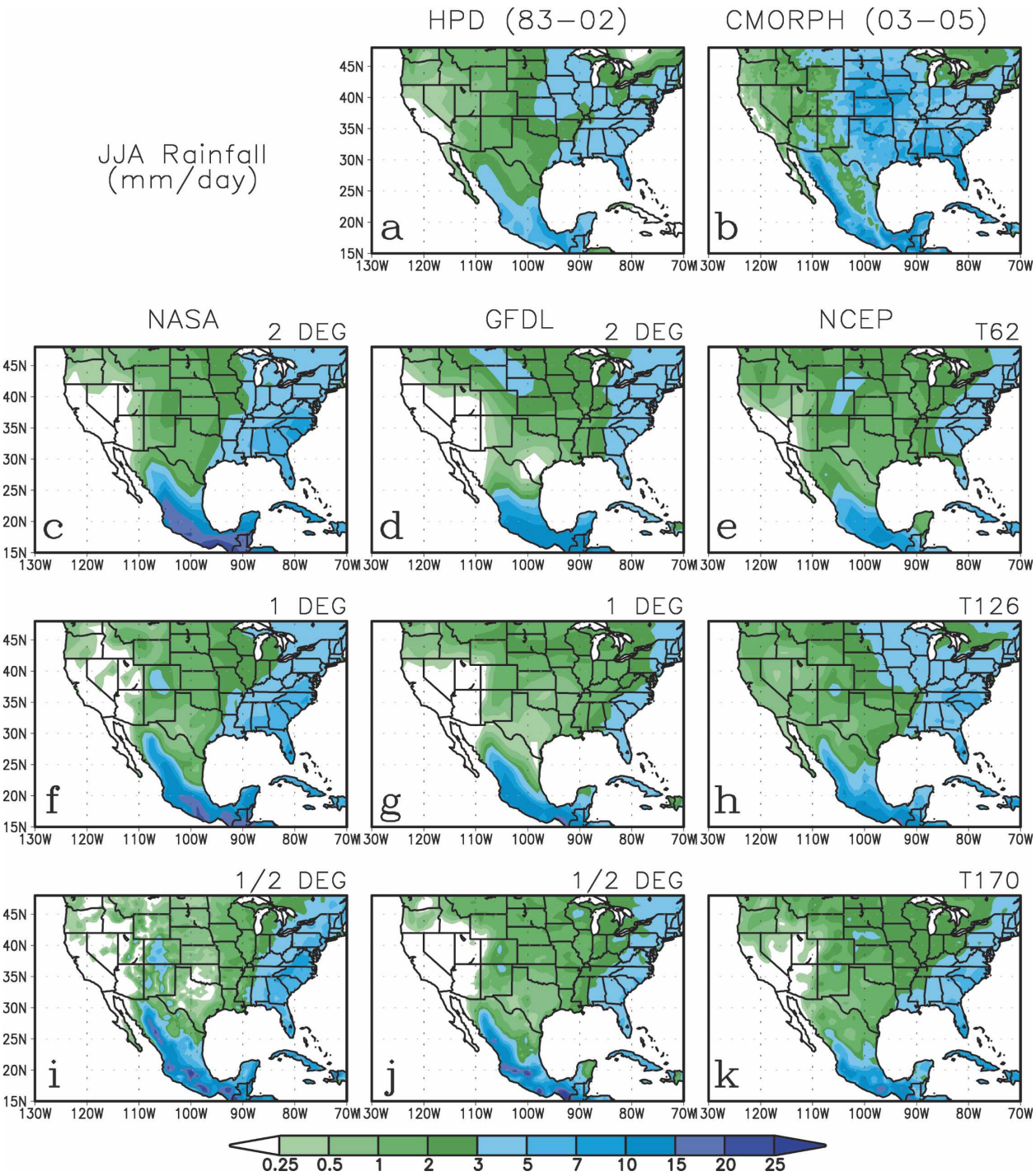

FIG. 1. Summer-mean (JJA) precipitation (mm day^{-1}) from the observations of the (a) NCEP/CPC 1° × 1° daily gridded precipitation analysis (average of 1983–2002) and (b) 1/4° × 1/4° CMORPH (average of 2003–05). (c)–(e) The model simulations in approximately 2°, (f)–(h) 1°, and (i)–(k) 1/2° horizontal resolutions [NASA simulations are shown in (c), (f), (i), GFDL in (a), (d), (g), (j), and NCEP in (b), (e), (h), (k)]. The model simulations are from the ensemble averages in each experiment. Values over the ocean points are masked out.

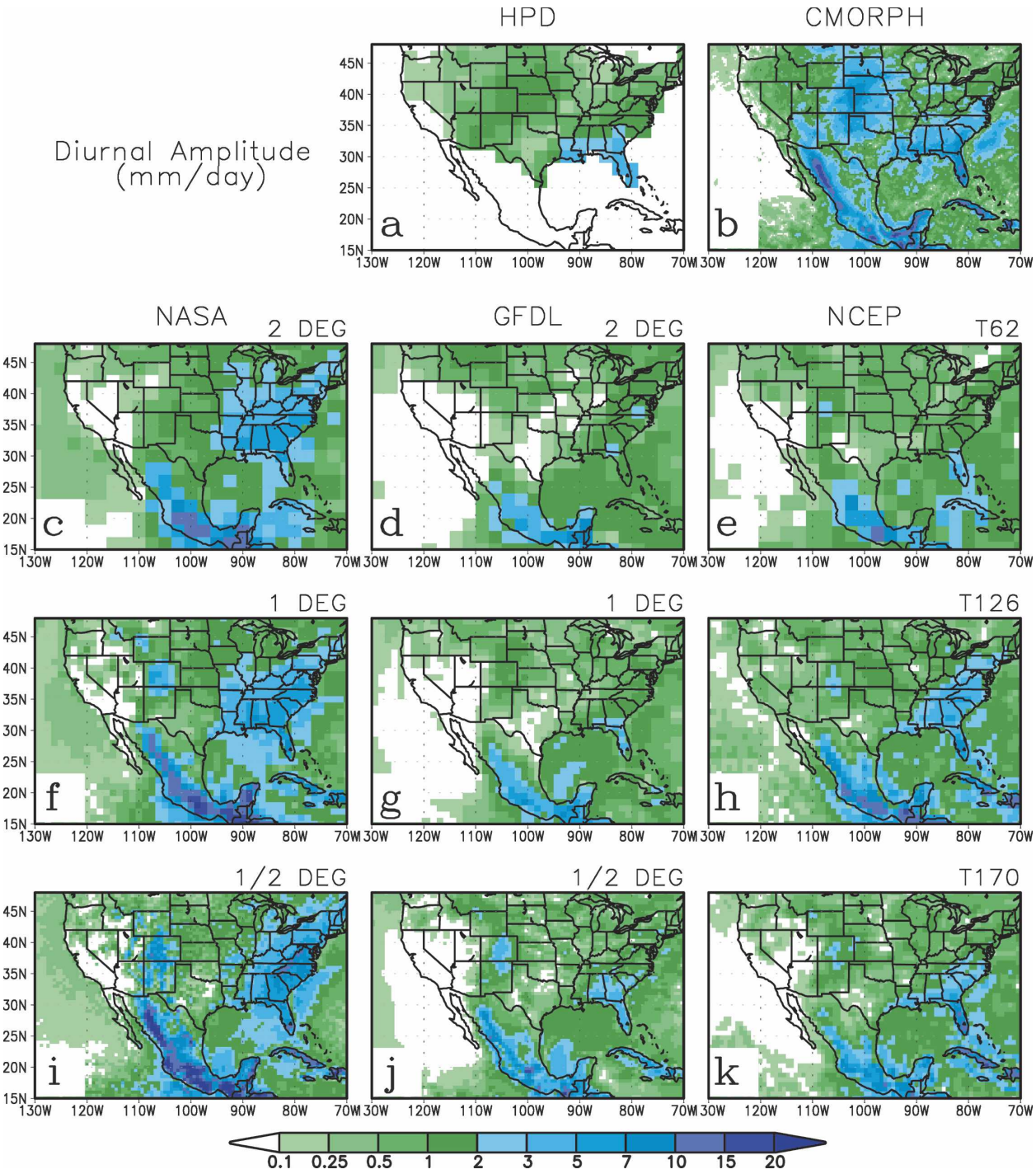

FIG. 2. Same as in Fig. 1 but for the amplitude of the diurnal cycle of precipitation (mm day^{-1}) from the observations and the model simulations. Observations are from (a) 20-yr (1983–2002) long-term statistics of 2° × 2.5° HPD and (b) the ¼° × ¼° CMORPH for the recent 3 yr (2003–05). The amplitude of the 24-h harmonic is given from the harmonic analysis applied to the JJA mean diurnal time series.

similar tendency to show an increase in amplitude over most of the continent, but less so in going from the T126 run to the T170 run. Compared with the T126 run, the T170 run shows a slight decrease in the diurnal amplitude over the southeastern United States. We find that in most cases, the simulated diurnal cycle amplitude increases with the seasonal-mean precipitation amount, especially over the North American monsoon

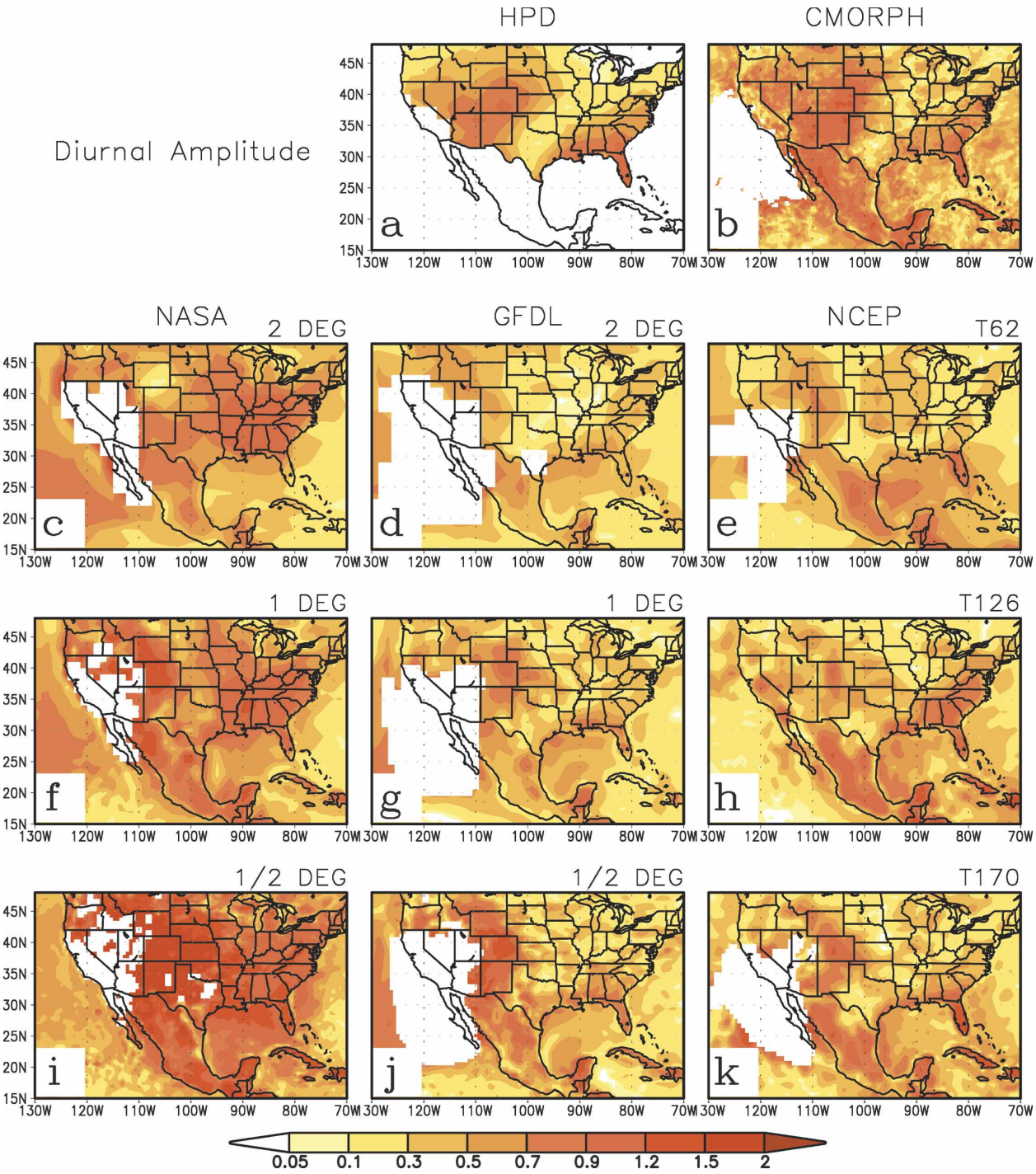

FIG. 3. Same as in Fig. 2 but the amplitude of the 24-h diurnal cycle is divided by the seasonal-mean precipitation. Areas of too-dry seasonal-mean precipitation less than 0.1 mm day^{-1} are masked out.

region and the southeastern United States. While the simulated diurnal variation over the ocean is much weaker than over the land regions, the higher-resolution runs show increased diurnal amplitudes over the coastal oceanic regions. For example, this occurs near the eastern and southern coasts of the United States and in southwestern Mexico (Fig. 2), probably as a result of the improved resolution of local land–sea breezes. Comparisons with the CMOPRH observations (Fig. 2b) suggest that these coastal features are realistic.

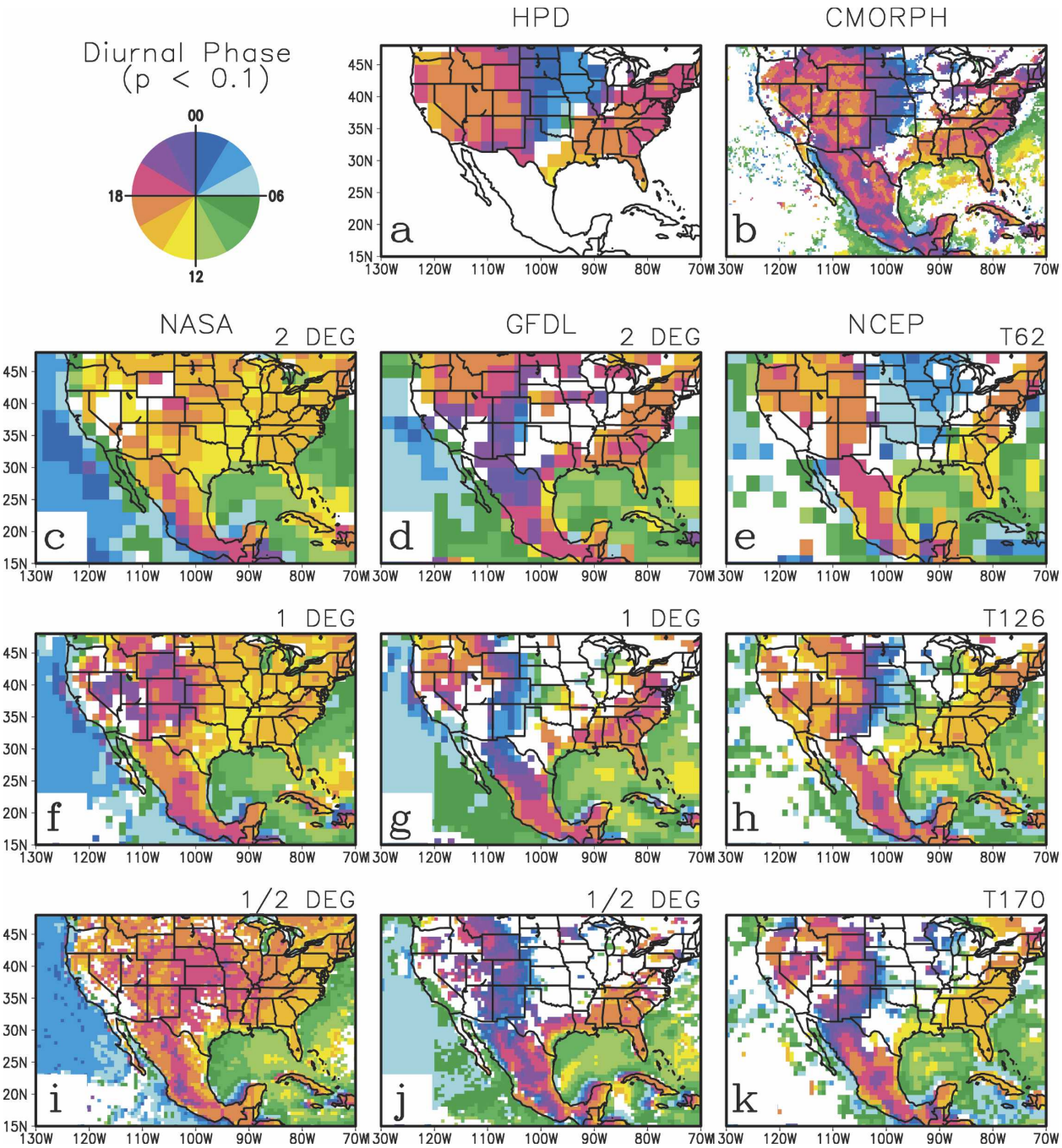

FIG. 4. Same as in Fig. 2 but for the local solar time (LST) of the maximum of the diurnal cycle of hourly precipitation. Only the statistically significant areas above the 90% confidence level are shaded in color.

We note that the amplitude of the diurnal cycle of precipitation also exhibits model dependencies, apparently as a result of the differences in the convection schemes. For example, the NASA model has stronger diurnal variations at all of the resolutions, compared with the GFDL and NCEP models. This appears to be primarily due to an overestimate in the convective buoyancy, resulting from a convective cloud base that is too close to the ground level in the NASA model (Lee et al. 2007).

b. *Phase*

Figure 4 shows the local solar time (LST) of the maximum in the diurnal cycle of rainfall. In the figure,

only the statistically significant areas above the 90% confidence level are shown. The significance test is described in the appendix. The HPD observations (Fig. 4a) exhibit the well-known feature of a late afternoon or evening maximum over most regions of the continent, except over the Great Plains where there is a nocturnal maximum in rainfall (e.g., Wallace 1975; Dai et al. 1999; Janowiak et al. 2007). Despite the coarse resolution of the HPD gridded rainfall data, the results show a clear evolution of the phase from just east of Rocky Mountains to the adjacent Great Plains and Midwest—a feature that is also evident in the high-resolution CMOPRH observations (Fig. 4b).

The three AGCMs exhibit large differences in the diurnal phase in the standard-resolution runs (cf. Figs. 4c, 4d, and 4e), which are described in detail by Lee et al. (2007). For example, the NASA model simulates afternoon rainfall maxima over most of the continents, except for evening maxima over the elevated regions of the SMO and Rocky Mountains. Generally, the model shifts the local time of the maximum 2–5 h earlier, compared with the HPD observations. As the model resolution increases, notable changes to the diurnal phase occur in the vicinity of the Rocky Mountains. The topographical influence seems to be better represented in the medium-resolution run (Fig. 4f), in which the model tends to simulate late afternoon to evening rainfall maxima (1600–2000 LST) on the top of the mountains (Colorado and the northern New Mexico) and nocturnal maxima (2000–2200 LST) in the surrounding area. Compared with the high-resolution CMORPH results, the eastward evolution of the phase is about correct over the region from Colorado to western Kansas, but it does not continue farther east to the adjacent plains as observed. Further increasing the resolution, however, does not result in further improvement in this case, with the high-resolution run (Fig. 4i) simulating a wide area of evening maximum on the downstream side and the adjacent plains. Over the rest of the continent, such as the southeastern United States and the North American monsoon region, the diurnal phase of the rainfall is rather insensitive to changes in resolution.

The GFDL 2° run (Fig. 4d) shows a realistic evening maximum in rainfall in the southeastern and northwestern United States—a feature that is largely insensitive to changes in model resolution. On the other hand, most of the nocturnal rainfall in the standard-resolution run is incorrectly located in the southwestern United States and northern Mexico, where the model has very dry biases in the seasonal-mean precipitation. Higher-resolution runs with the GFDL model exhibit significant changes over the Rocky Mountains, especially in the ½° run (Fig. 4j) in which the phase appears to be locked more to the topographical features. There is a hint of an eastward phase transition over the eastern slope of the Rocky Mountains, although it does not extend east of 100°W as observed. The nighttime precipitation tends to occur between local midnight and early morning over most of the Great Plain, but these signals are spatially less organized and statistically not significant (masked out in the figures). In general, the GFDL model exhibits a maximum in the diurnal cycle of precipitation over the top of the Rocky Mountains at around 2000–2400 LST, which is several hours later than that found in the observations.

Unlike the other two models, the NCEP 2° run (Fig. 4e) produces nighttime rainfall after local midnight in a wide area of the midcontinent between the Rocky Mountains and the Appalachians. Lee et al. (2007) discussed that this feature in the NCEP model is primarily related to the differences in the parameterized convection scheme. In particular, the NCEP scheme includes a dynamical trigger mechanism for the development of deep convection that is a function of the vertical motion at the top of the boundary layer. The resolution increase in the NCEP model has little influence on the large-scale phase patterns. For example, over the southeastern United States, the simulated rainfall reaches its maximum in the early afternoon (about 2 h earlier than in the observations), regardless of the model resolution. The model also captures the evening maximum of rainfall over the Rocky Mountains and the western United States. However, the higher resolution does improve regional-scale features such as the phase transition from the Rocky Mountains to the Great Plains (e.g., T126 run shown in Fig. 4h).

The three models all show some improvement in the oceanic diurnal cycle of rainfall with increasing resolution. Combined with the increased amplitude of diurnal rainfall, the higher-resolution runs tend to capture better the coastal phase transition along the Atlantic, the northern Gulf of Mexico, and along the eastern Pacific southward to Baja California. These features are consistent with the high-resolution CMORPH observations, where the local time of the maximum is generally delayed from early morning to afternoon as one moves away from the coast. It is likely that the improved resolution of local orography, land–ocean contrast, and the curvature of the coastlines all contribute to the better representation of the propagation of land-initiated diurnal convection (Yang and Slingo 2001; Janowiak et al. 2007) and the diurnal migration of land–sea-breeze fronts (Tian et al. 2005). Both the CMORPH observations and the models show the general pattern of early morning precipitation maxima over the adjacent oceans in contrast to the afternoon and evening maxima over

the land areas. Previous studies suggest the presence of large-scale thermally driven diurnal circulation (Silva Dias et al. 1987; Dai and Deser 1999; Dai 2001) in which the deep convection over the land in the afternoon and early evening induces the compensating subsidence over large nearby oceanic areas to suppress the convection. The opposite occurs in the early morning.

The estimate of the observed diurnal cycle is significant at most grid points, whereas the model simulations show large regions where it is not significant. This is especially true over the Great Plains and for those models (especially GFDL) that show a tendency for a nocturnal maximum. The lack of significance in the Great Plains likely reflects the irregular nature of the mechanisms driving the diurnal cycle in that region (e.g., eastward propagation of convective systems and nocturnal moisture transport by low-level jet): these mechanisms are either not adequately simulated and/or the smaller sample size of the simulations is insufficient to produce significant estimates. In contrast with the other two models, the NASA model results are significant in most regions and at all resolutions, reflecting an unrealistically strong control by local thermodynamic processes on the diurnal cycle in that model.

While there are no major broad-scale improvements over the continental region with increasing resolution, there are nevertheless some regional aspects to the diurnal cycle simulations that have improved and warrant further investigation. For example, we have seen some evidence for improvements in the phase of the diurnal cycle of rainfall over the Rocky Mountains and adjacent Great Plains, possibly as a result of resolving mountain-initiated mesoscale convective systems. The high-resolution runs also show some signature of downslope propagation of mountain-initiated convective systems in the North American monsoon region over the western slope of the SMO and the Gulf of California. These highly model-dependent improvements will be examined in more detail in the next section.

5. Regional diurnal cycle simulations

a. Great Plains

The summertime diurnal cycle of precipitation over the Rocky Mountains–Great Plains region (30°–45°N, 115°–85°W) shows two distinct features: an eastward-propagating maximum between 105° and 90°W and a stationary maximum to the east (90° and 80°W). Figure 5 (left column) shows this behavior based on the NARR data. The figure shows the climatological-mean (1983–2002 average) diurnal cycle of precipitation and low-level winds at 925 hPa over the region. The NARR results are not qualitatively different from those based on the low-resolution HPD data (cf. Fig. 13 of Lee et al. 2007) or the high-resolution CMORPH observations.

The precipitation is initiated over the mountains in the afternoon, peaking around 1800 LST (0000 UTC). The convection center then migrates eastward, with a maximum of rainfall over the eastern slope of the mountains shortly before midnight (0600 UTC) and over the Great Plains east of 100°W after midnight and into the early morning hours, which is consistent with mountain-initiated systems propagating eastward (Carbone et al. 2002; Tian et al. 2005; Janowiak et al. 2007). The other region with a strong diurnal variation in rainfall is east of 90°W, where we see a stationary maximum between late afternoon and evening (2100–0000 UTC). This is accompanied by a broad-scale diurnal variation over the eastern part of the continent, as discussed in the previous section (Fig. 4). We will focus here on the regional features of the Rocky Mountain–Great Plains variability to the west of 90°W.

Figure 5 (left column) also shows the diurnal departures of the NARR low-level winds associated with these precipitation features. Over most of the plains, the diurnal variation of low-level winds shows a clockwise rotation, with northerlies in the daytime and southerlies in the nighttime. The precipitation clearly intensifies in the downslope region and the adjacent Great Plains, where the nighttime (0900 UTC) maximum of rainfall occurs at a time of maximum southerly flow associated with the nocturnal Great Plains low-level jets. The important role of this flow in supplying the moisture for the nighttime precipitation over the Great Plains has been discussed in many studies (e.g., Helfand and Schubert 1995; Higgins et al. 1997; Schubert et al. 1998).

The climatological-mean diurnal cycles of precipitation and 925-hPa winds for the three model simulations and for the three different horizontal resolutions are presented in Fig. 5 for the NASA model, Fig. 6 for the GFDL model, and Fig. 7 for the NCEP model. At each resolution, the NASA model generates rainfall that begins over the mountains at 1800–2100 UTC, which is roughly consistent with the reanalysis but much stronger, particularly at the higher resolutions. In general, increasing the model's horizontal resolution tends to produce more daytime rainfall and greater dryness during the rest of a day. Unlike the lower-resolution runs, the ½° run simulates a rapid downslope expansion of rainfall to the adjacent plains during local evening (around 0000 UTC; also inferred from Fig. 4i). This feature will be discussed later in more detail. On the other hand, the diurnal variation of the low-level winds is quite good at all resolutions. For example, the model

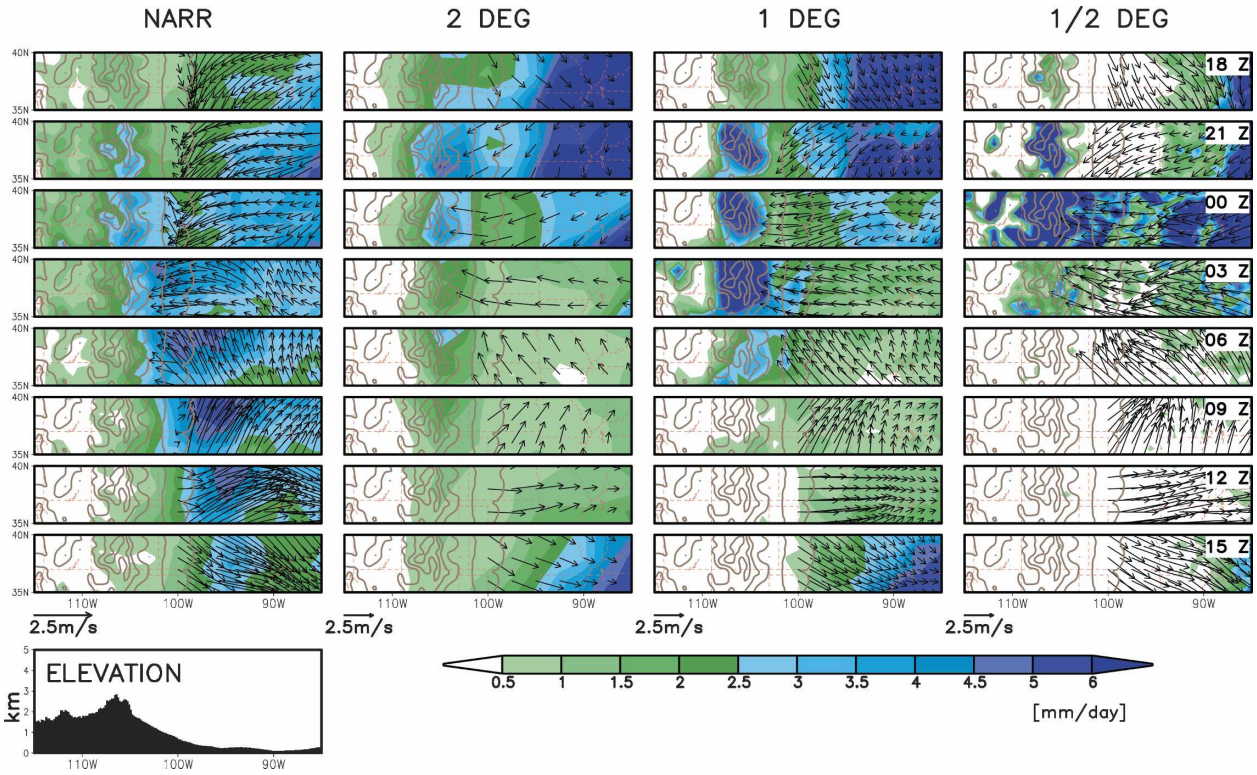

FIG. 5. Mean precipitation (mm day^{-1}, shaded) and 925-hPa wind (m s^{-1}, arrow, diurnal departure from the daily mean) in 3-h interval over the Rocky Mountains–Great Plains region (30°–45°N, 115°–85°W) from the NARR (first column) and the NASA model simulations in 2° (second column), 1° (third column), and ½° (forth column) horizontal resolution. Winds below the ground level are masked out. The surface elevation is shown together in each panel (contoured in brown) at a 0.5-km interval, and the mean surface elevation in 35°–40°N latitude belts (in km scale) is illustrated in the bottom-left panel.

captures well the nocturnal southerly flows (0600–0900 UTC) associated with the low-level jets. This implies that the parameterized precipitation process in the model is rather insensitive to the large-scale wind variations and accompanying moisture flux, regardless of the model resolution. This is apparently a typical problem of buoyancy closure convection schemes (Lee et al. 2007).

An increase in the resolution of the GFDL model also induces much stronger diurnal rainfall variability over the mountain region (Fig. 6). One of the notable differences, however, is that the higher-resolution runs have a hint of the downslope movement of the precipitation. Compared with the observations, the eastward movement is quite slow and the propagation signal is too confined to the slope region. In terms of the eastward propagation, the NCEP model shows a clear improvement in the higher-resolution runs (Fig. 7). At low resolution, the rainfall maximum remains over the high topography throughout the day, with only a hint of downslope movement at night. The higher-resolution runs, particularly the T126 case, show a clear eastward propagation, with a nighttime maximum at 0900 UTC over the plains. Even the best case, however, is still unrealistic in that the strongest precipitation occurs over the mountains in the afternoon (2100 UTC).

To gain further insight into the nature of the eastward propagation of the convection systems, we examined the individual rainfall events in the observations and the highest-resolution model simulations. Figure 8 shows Hovmöller diagrams of the meridionally averaged (30°–40°N) precipitation for selected 15-day periods from the CMORPH data and the three model simulations. We selected typical periods of strong diurnal variations in rainfall over the Rocky Mountains and the adjacent Great Plains. In the CMORPH data, we see a clear eastward-propagating signal of the diurnal convection systems extending from the mountains to the adjacent plains. Many (but not all) of the rainfall events in the Great Plains are associated with eastward-migrating rainfall systems, which is consistent with the findings of Carbone et al. (2002). These observed propagation characteristics are most apparent from June to mid-July.

To a large degree, the above Hovmöller results are consistent with the climatological-mean diurnal cycle

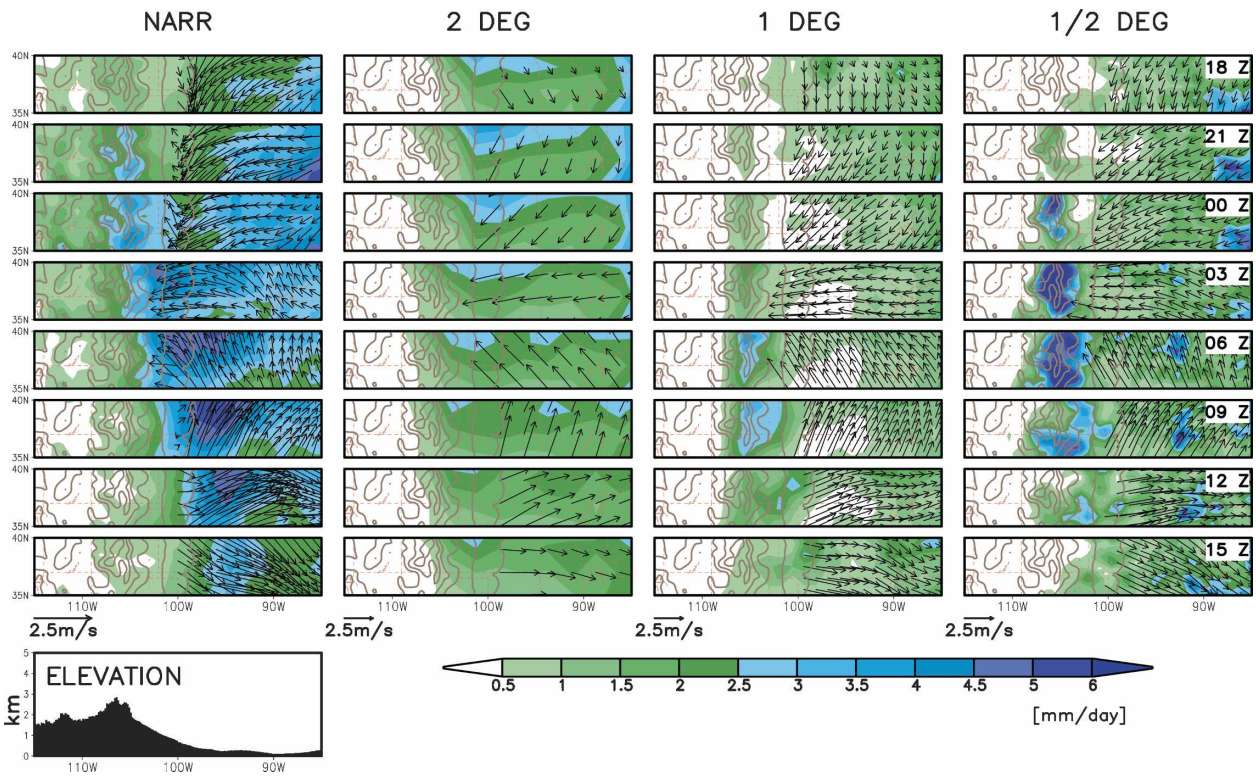

FIG. 6. Same as in Fig. 5 except for the GFDL model simulations in 2° (second column), 1° (third column), and ½° (forth column) horizontal resolution.

patterns shown in Figs. 5–7. The NASA model is characterized by a very regular diurnal cycle of convection in the mountains. The lifetimes of individual precipitation events are relatively short, compared with the CMORPH observations and the other two AGCMs. The GFDL and NCEP models, on the other hand, do show some eastward propagation from the mountains. However, the propagation speed in the GFDL simulations is too slow, whereas the NCEP model shows more realistic propagation speeds.

We speculate that the different propagation speeds of the convective systems are related to model differences in the vertical structure of the diabatic heating induced by latent heat release (Gill 1980; Silva Dias et al. 1987). If we consider a shallow water model, shallower vertical heating should be more favorable to stationary convective systems (slow modes with small equivalent depth), whereas deep heating should be more favorable to faster propagation (fast modes). In that regard, the large-scale condensation scheme in the model effectively produces a shallower heating structure and, therefore, more stationary systems. Therefore, it would be interesting to see how the models partition total precipitation into deep convective rainfall and the large-scale condensation. Figure 9 compares the ratio of the convective to the total precipitation amount in the three models at the three different resolutions. As the model resolution increases, the models generally tend to simulate less precipitation from the deep convection scheme. There are notable differences among the models. The large-scale condensation scheme plays a larger role in the GFDL and NCEP models than in the NASA model, particularly over the Rocky Mountains–Great Plains region. In the high-resolution runs, and focusing on the seasonal-mean rainfall patterns (shown in Fig. 1), the GFDL model simulates the largest contribution to the precipitation from the grid-scale condensation process (and exhibits slow propagation), whereas the NASA model simulates the smallest amount (fast propagation). The contribution in the NCEP model is in between that of the other two models, and the model exhibits moderate propagation speed.

b. North American monsoon region

In the North American monsoon region we will focus our attention on the highest-resolution runs (½°, T170), for which most of the complex terrain over the North American monsoon tier-1 region (Higgins et al. 2006) is fairly well resolved. These runs are validated against

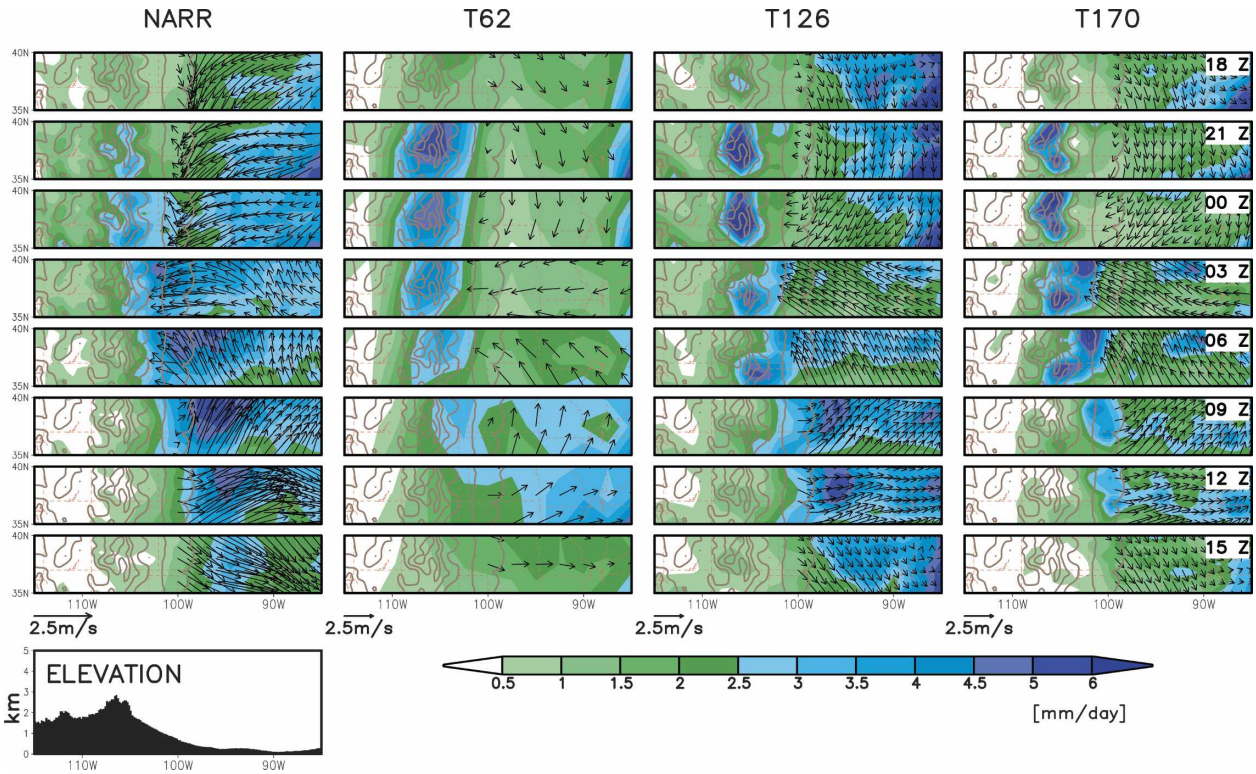

FIG. 7. Same as in Fig. 5 except for the NCEP model simulations at T62 (second column), T126 (third column), and T170 (forth column) horizontal resolution.

observations from satellites and in situ NAME observations at fine horizontal resolution.

We first compare the fine structure of the North American monsoon simulations. Figure 10 compares the JJA mean precipitation over the NAME region from observations (CMORPH, averaged over 2003–05) and the simulations (ensemble means). The figure also compares the simulated seasonal-mean low-level winds with those from the NARR data (average of 1983–2002). The observations show the typical structure of the monsoon rainband, an elongated maximum oriented in a NW–SE direction extending from central Mexico into the southwest United States along the SMO. At the northern end of this region, the main monsoon rainband connects to a secondary maximum over Arizona and New Mexico that is also associated with topography. In the observations, the rainfall peaks over the southwestern, windward slope of the mountains.

All three models simulate the two topographic rainfall maxima, but all three show serious deficiencies. The NCEP model, which is at slightly lower resolution than the other two, barely captures the main monsoon rainband, and none of the models properly simulate its northward extent into the U.S. southwest. The models are more consistent with the topographic rains over Arizona and New Mexico, although they are much weaker than observed. In comparing the rainfall magnitude with these observations, however, we should bear in mind the possible positive bias of the satellite estimates over the land (Janowiak et al. 2007). The NASA model produces the strongest monsoonal rainfall, even stronger than the satellite estimate in the central SMO. Its precipitation maximum, however, lies along the peak of the topography, rather than on the western slope, as is found in the observations. This is consistent with its behavior in the Great Plains case, where it also tended to lock the precipitation over the highest topography.

Although the quality of the upper-air assimilation in the NARR may be affected by the paucity of vertical soundings in this region, the analyzed winds are clearly responding to land–sea contrasts along the gulf and Baja California, as well as to the topography along the SMO. Offshore we have west-northwesterly flows associated with the Pacific anticyclone, turning to a southerly monsoon inflow all along the eastern gulf shore. This results in strong upslope flow along the western

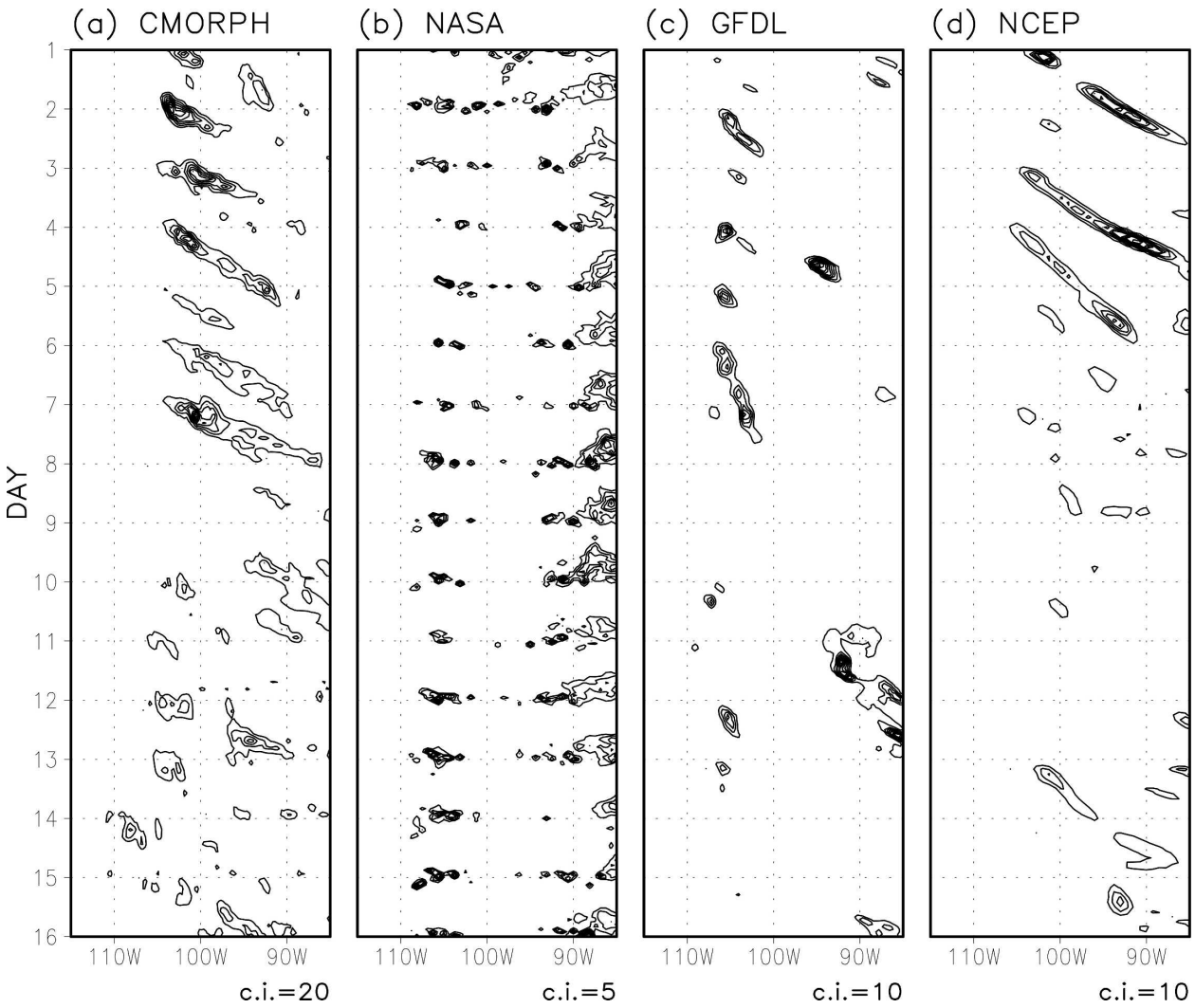

FIG. 8. Hovmöller diagrams (115°–85°W) of precipitation rate (mm day^{-1}) averaged over 30°–40°N, from (a) the CMORPH observations, along with the simulations by the (b) NASA, (c) GFDL, and (d) NCEP models. The observations are shown for the period of 0000 UTC 16 Jun–0000 UTC 1 Jul 2004 from the 3-hourly dataset. The time periods are different among the models and consist of an arbitrary span of 15 days in the summer (JJA) from hourly outputs.

SMO. In this region, unlike the Great Plains discussed above, the models fail to capture the main features of the low-level flow pattern. In particular, they have great difficulty in turning the northwesterly large-scale flow into the monsoon region.

The observed diurnal cycle of rainfall over the NAME tier-1 region was constructed from NERN precipitation estimates. This dataset provides a high temporal (hourly) sampling rate that allows an accurate estimate of the diurnal cycle over the region; its spatial coverage, however, is limited to the northwestern Mexico area where most of the instruments are installed (Gochis et al. 2004). Figure 11 compares the local time of maximum for the diurnal cycle of precipitation from the NERN observations and the three model simulations. The NERN observations show a phase transition in time, depending on the surface elevation, that is quite similar to that found on the eastern slope of the Rocky Mountains and the adjacent plains. At the highest elevations, diurnal convection reaches a maximum in the late afternoon (1400–1600 LST), which gets gradually delayed as one moves down the slope, with an evening maximum on the slope and a near-midnight maximum close to the gulf.

The NASA model shows a clear separation of the phase of the diurnal cycle between land and ocean, with daytime (late afternoon to evening) convection dominating over land and nighttime convection dominating

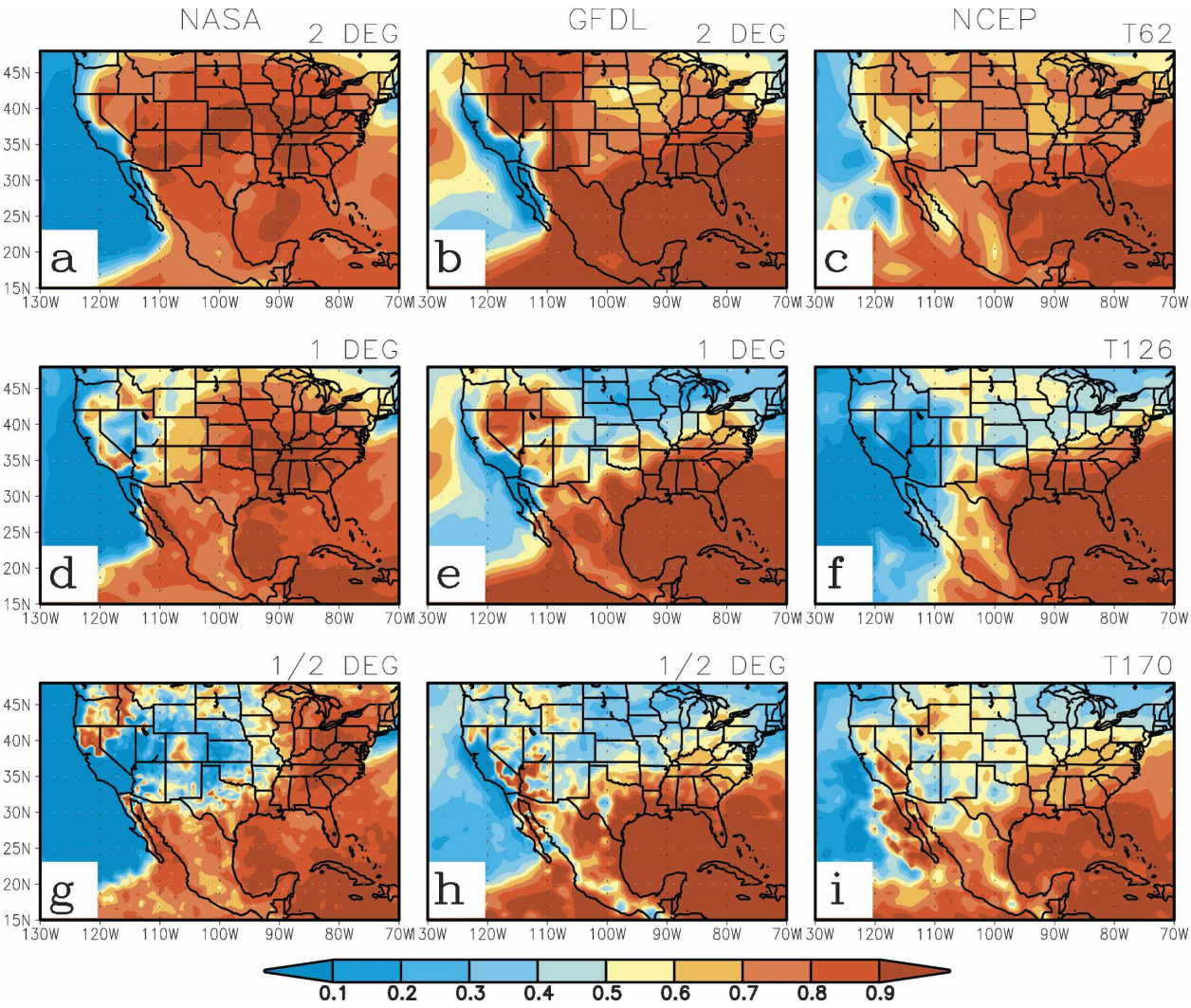

FIG. 9. The ratio of convective precipitation to the total precipitation amount in the three models at the three different horizontal resolutions.

over the ocean, but it shows none of the observed effects of topography. The other two models, on the other hand, capture the phase changes along the western slope of the SMO. Compared to the observations, the timing of the maximum is delayed a few hours in both models, with late development of convection on top of the mountains, and a convection maximum after midnight near the gulf coast.

To examine further the phase difference in diurnal rainfall maxima, we examined the climatological-mean spatial pattern of the diurnal cycles of precipitation and low-level winds in a small region on the western slope of the SMO (24.5°–25.5°N and 111°–105°W), which is illustrated in Fig. 12. The CMORPH observations show a clear westward propagation of precipitation down the western slope of the SMO. Rainfall intensity maximizes between late evening and midnight in the slope region, weakening as it enters the gulf in the early morning (1200–1500 UTC or 0500–0800 LST). The diurnal variation of the NARR low-level wind anomalies over the slope region consists of a clockwise rotation, with an upslope departure toward the east developing from late afternoon to evening (2100–0300 UTC) and a downslope departure toward the ocean after midnight (0600–1500 UTC).

Consistent with the phase map in Fig. 11, the NASA model shows little movement of the rainfall, but it exhibits a diurnal shift between the daytime maximum precipitation over the land in late afternoon to early evening, and nighttime maximum over the ocean between midnight and morning. The GFDL model simulation shows systematic westward propagation in the precipitation. The model captures the maximum in the rainfall intensity along the slope similar to the

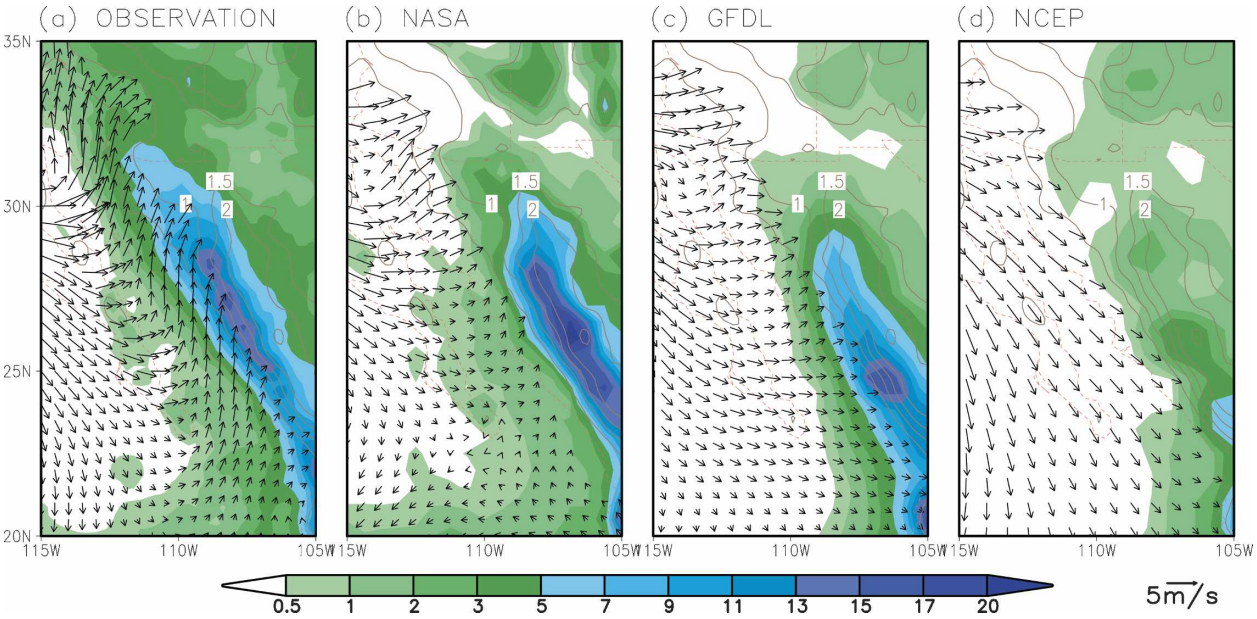

FIG. 10. Summer-mean (JJA) precipitation (mm day^{-1}, shaded) and 925-hPa wind (m s^{-1}, arrow, masked out below the ground level) over the NAME tier-1 region (20°–35°N, 115°–105°W). (a) The observed CMOPRH precipitation (2003–05) along with the NARR winds, and (b)–(d) the three model simulations at 1/2° horizontal resolution (T170 run for the NCEP model). Contours indicate the surface elevation at the 0.5-km level.

CMORPH observations, but the westward movement is somewhat slow with the maximum at 0900 UTC. The slow movement is consistent with the model behavior on the eastern slope of the Rocky Mountains. In the model, we find that precipitation from large-scale condensation dominates on the western slope of the SMO (Fig. 9h), which again suggests a possible relationship between the vertical heating structure and the propagation speed. The NCEP model also shows a hint of downslope propagation of rainfall, although it is not as clear as in the GFDL model, perhaps due to the very small magnitude of the rainfall simulated by the NCEP model in that region.

In all three models, the simulated diurnal variations

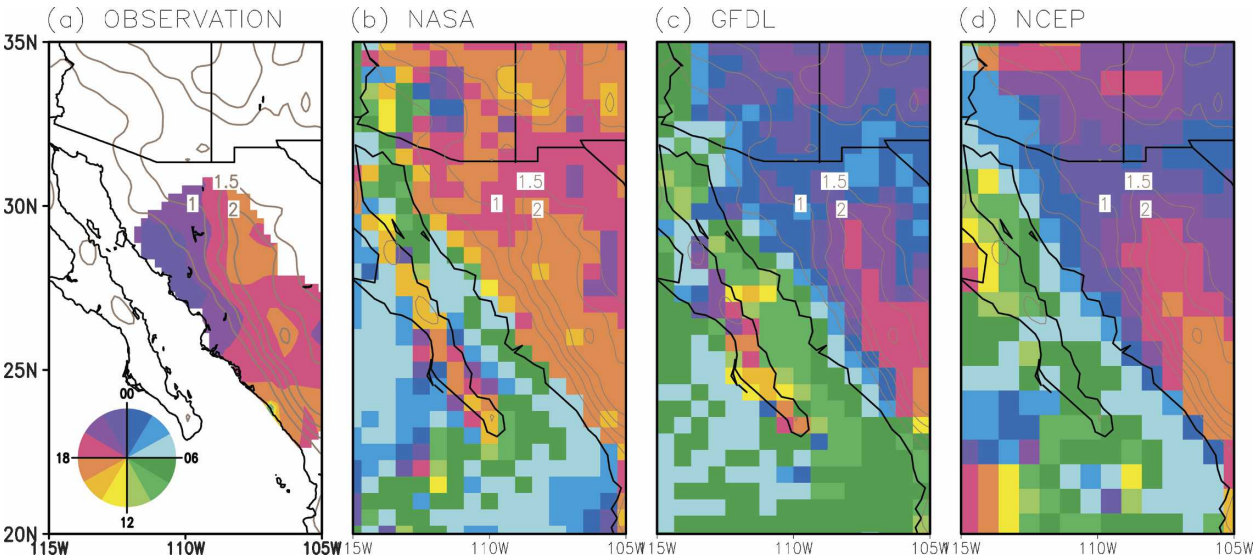

FIG. 11. LST of the maximum of the diurnal cycle of the hourly precipitation over the NAME tier-1 region. (a) The NERN observation, and (b)–(d) the three model simulations at ½° horizontal resolution (T170 run for the NCEP model). The surface elevation is contoured.

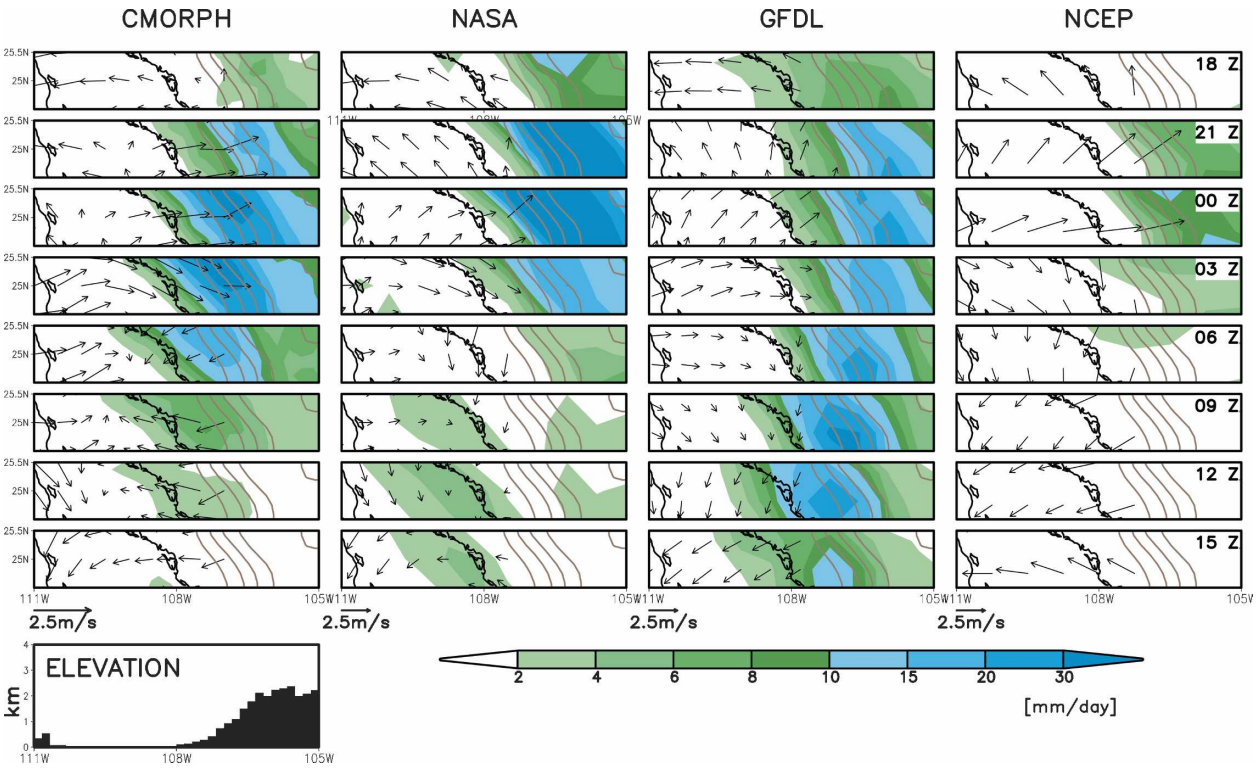

FIG. 12. Mean precipitation (mm day^{-1}, shaded) and 925-hPa wind (m s^{-1}, arrow, masked out below the ground level) at 3-h intervals over the western slope of the SMO and the Gulf of California region (24.5°–25.5°N, 111°–105°W) from the CMORPH observations and the NARR reanalysis wind (first column), and the model simulations at 1/2° resolution from the NASA (second column), the GFDL (third column), and the NCEP (forth column) models. The surface elevation is shown together in each panel (contoured in brown) at 0.5-km intervals, and the mean surface elevation between 24.5° and 25.5°N (at km scale) is illustrated in the bottom-left panel.

of low-level winds show upslope flow in the evening and downslope flow after midnight. The NASA model simulates relatively weaker nighttime downslope winds, whereas the NCEP model simulates relatively stronger downslope winds during the night.

6. Conclusions

In this study we examined the impact of horizontal resolution on the North American warm season diurnal cycle of precipitation in three AGCMs (those of NASA/GMAO, GFDL, and NCEP). Ensembles of simulations were done for the warm season at a typical climate model resolution of about 2° latitude–longitude, and compared with additional ensembles of runs that differ only in the model resolution (about 1° and ½°). The simulations were validated against the reanalysis data from the NARR, the HPD hourly gridded (2° latitude × 2.5° longitude) gauge precipitation dataset, the satellite-derived CMORPH precipitation data (¼°), and the NERN rain gauge dataset over the North American monsoon region.

Increased resolution was found to have mixed impacts on the diurnal cycle of precipitation, especially for the phase. In the higher-resolution runs, the models begin to resolve the late-day and nocturnal rainfall on the downstream side of the Rocky Mountains and the adjacent Great Plains. Similar improvements were found on the western slope of the SMO in the region of the North American monsoon. These improvements appear to be mostly the result of a better representation of the downslope propagation characteristics of the convective signal initiated over the mountains (Maddox 1980; Riley et al. 1987; Carbone et al. 2002). The improvements are, however, model specific, with the NASA model showing the least sensitivity to resolution changes. On the other hand, all the models improve the oceanic diurnal cycle of rainfall adjacent to the continent, where the models capture the correct phase transition from early morning to afternoon as one moves away from the coast. The latter improvements are apparently due to the better representation of local land–sea breezes and the large-scale thermally driven land–ocean circulations.

While some eastward-propagation characteristics are captured in the higher-resolution runs over the Great

Plains, the propagating signals for the most part do not extend beyond the slope region of the Rocky Mountains, and this exacerbates a tendency for the models to dry out in the Great Plains. Another reason for the dry bias over the Great Plains appears to be the result of a too strong coupling of the convection schemes to the surface and the resulting lack of sensitivity of the convection to large-scale dynamic forcing, such as that associated with the nocturnal low-level jets (Zhang 2003; Lee et al. 2007) and large-scale vertical motion (Dai et al. 1999): this problem exists regardless of the model resolution. The NCEP model is, however, an exception in that it does simulate realistic nocturnal rainfall over the Great Plains–Midwest at all the resolutions considered here. This appears to be the result of a dynamical trigger in the deep convection scheme that depends explicitly on the vertical motion at the top of the PBL (Lee et al. 2007).

Several deficiencies in the simulated diurnal cycle of precipitation warrant further investigation into the model physics that is responsible for the convection and precipitation processes. Over the mountains, the models tend to have a too strong diurnal variation of rainfall producing a wet bias that is worsened as the precipitation becomes more strongly phase-locked to the high terrain with increased resolution (most evident in the NASA model). The reason for this strong locking of rainfall to the mountains is not clear. One possible explanation involves the convective instability of the second kind (CISK) type destabilization induced by too strong convection in the model. The accompanying strong regional compensating subsidence might suppress the convection around the local convection maximum (top of the mountains in this case) and produce highly localized ("bull's-eyed") precipitation patterns. This mechanism seems to be operating in the NASA model, in view of the fact that most of the mountain rain is produced by the deep convection scheme. In fact, we found that the fraction of convective rainfall to the total precipitation amount varies widely among the models. The two models with less convective rainfall (GFDL and NCEP) do tend to simulate more nocturnal rainfall over the Great Plains, though the timing of the maximum is not very robust. One explanation for the differences associated with the large-scale and convective schemes is that the large-scale condensation scheme is less tied to the regular diurnal variation of near-ground heating in the PBL, and more responsive to the large-scale flows, such as the nocturnal low-level jets. We also suggest that the ratio of convective to large-scale heating should be important for correctly simulating eastward-propagating convective systems and their propagation speeds, in that it affects the vertical structure of diabatic heating.

Although we have found that some improvements in the representation of the diurnal cycle in precipitation can be achieved by simply increasing the resolution, the inability to properly reproduce the regional characteristics in amplitude and phase appears to be primarily due to the problems in the model physics that are largely unrelated to resolution. In that regard, this study highlights the need for further improvements to the parameterization of moist convection processes.

Acknowledgments. We thank Aiguo Dai and Pedro L. Silva Dias and two anonymous reviewers for their helpful comments. We are grateful to Dave Gochis for providing the NERN precipitation dataset through the UCAR/JOSS Web site. This study was sponsored by NOAA's Office of Global Program's GEWEX Americas Prediction Project/Pan American Climate Studies (PACS/GAPP) North American Warm Season Precipitation Initiative.

APPENDIX

Estimation of Sampling Error in Diurnal Cycle Fits

Our method of estimating the amplitude and phase of the model-generated diurnal cycle of precipitation is based on fitting the model data at each grid point to a Fourier series. The statistical significance of the cycle amplitudes is determined from the variance of the coefficients of daily fits to the data, following a procedure described in Bell and Reid (1993). The method is similar to one used by Collier and Bowman (2004). Given the time series $R(t_i)$ for rain rate in a given box at times t_i, we suppose a climatological-mean diurnal cycle $r(t)$ as a function of hour of the day t. It can be described as

$$r(t) = r_0 + \sum_{n=1}^{M} r_n \cos[\omega_n(t - \phi_n)], \qquad \text{(A.1)}$$

where r_0 is the climatological-mean rain rate and the ω_n is the angular frequencies represented as

$$\omega_n = 2\pi/(n \times 24\text{h}). \qquad \text{(A.2)}$$

The "diurnal cycle" is sometimes defined to be the amplitude and phase r_1, φ_1 of the $n = 1$ sinusoid, and the "semidiurnal cycle" is defined by the amplitude and phase r_2, φ_2. We will refer to these components more generally as the "n cycle." In principle, we can use the data to estimate $r(t)$ by obtaining the average of $R(t_i)$ for each hour of the day t, and then getting the Fourier components of this average.

The significance of estimated amplitude and phase of the diurnal cycle can be tested by basically describing

the diurnal cycle in terms of Fourier components in each day of sampling and examining their spread or variance in time. For doing this, we first need to convert Eq. (A.1) into a linear least squares problem. To do the fitting with the linear least squares procedure, Eq. (A.1) is rewritten as

$$r(t) = r_0 + r_{1c}\cos(\omega_1 t) + r_{1s}\sin(\omega_1 t) + \cdots, \quad \text{(A.3)}$$

with

$$r_{nc} = r_n \cos(\omega_n \phi_n),$$
$$r_{ns} = r_n \sin(\omega_n \phi_n). \quad \text{(A.4)}$$

Using these estimates we can describe the uncertainty in the n-cycle amplitude and phase. The n cycle is now described by the two-component vector in Eq. (A.4), $\{r_{nc}, r_{ns}\}$, which has length r_n and orientation φ_n (in h). If we describe departures from the estimated n-cycle vector by $\{\delta r_{nc}, \delta r_{ns}\}$, then we can use the standard deviations of the error to describe the probability distribution of possible departures $\{\delta r_{nc}, \delta r_{ns}\}$ from the n-cycle vector estimate as

$$\Pr(\delta r_{nc}, \delta r_{ns}) = \frac{1}{2\pi\sigma_{nc}\sigma_{ns}} \exp\left\{ -\left[\frac{(\delta r_{nc})^2}{2\sigma_{nc}^2} + \frac{(\delta r_{ns})^2}{2\sigma_{ns}^2} \right] \right\}, \quad \text{(A.5)}$$

where we are denoting the uncertainties in the cosine and sine components of the n cycle by σ_{nc} and σ_{ns}, respectively, which are calculated from the standard deviations for r_{nc} and r_{ns} from the daily fits. By assuming that the error variances of σ_{nc}^2 and σ_{ns}^2 are very close to each other, we can use Eq. (A.5) to obtain the probability that the vector describing the n cycle lies within a probability circle of radius δr_n defined as

$$\delta r_n = \sqrt{(\delta r_{nc})^2 + (\delta r_{ns})^2}. \quad \text{(A.6)}$$

The distribution of the radius of errors is obtained from the vector distribution (A.5) by integrating over the angle of the error vector, and is given by

$$\Pr(\delta r_n > \delta r) = \exp\left\{ \frac{-(\delta r)^2}{\sigma_n^2} \right\}, \quad \text{(A.7)}$$

where we have defined

$$\sigma_n^2 \equiv \sigma_{nc}^2 + \sigma_{ns}^2. \quad \text{(A.8)}$$

If, for instance, we want to define the circular region within which the n-cycle vector lies with 90% confidence, its radius is obtained by solving (A.7) with $p = 0.1$:

$$p = \exp[-(\delta r)^2/\sigma_n^2]$$
$$\delta r(p) = \sqrt{-\ln p}\,\sigma_n. \quad \text{(A.9)}$$

The radius of the 90% confidence limit circle is, in particular,

$$\delta r(0.1) = 1.51\sigma_n. \quad \text{(A.10)}$$

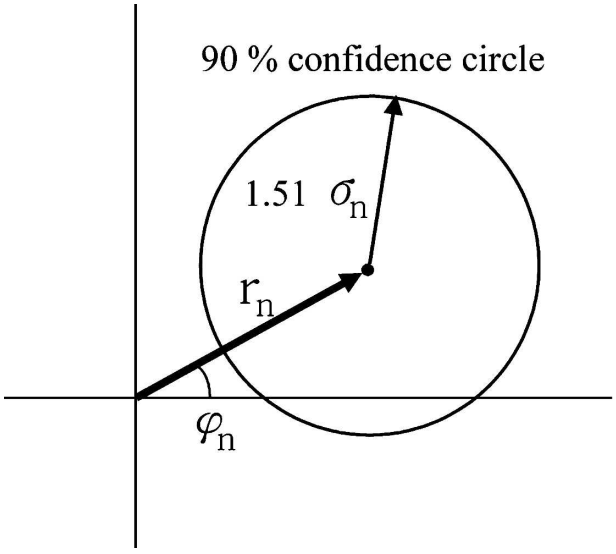

FIG. A1. Vector (amplitude and phase) of the n-cycle component of diurnal variation, and confidence limits for the vector as determined from Eq. (A.10).

Figure A1 shows a schematic of the 90% confidence-limit circle for an n-cycle fit. It is regarded as significant only if the length of the n-cycle vector exceeds the radius of the 90% confidence-limit circle.

REFERENCES

Anderson, J. L., and Coauthors, 2004: The new GFDL global atmosphere and land model AM2/LM2: Evaluation with prescribed SST simulations. *J. Climate,* **17,** 4641–4673.

Arritt, R. W., and M. J. Mitchell, 1994: Variability of the Great Plains low-level jet and its influence on mesoscale convection. Preprints, *Sixth Conf. on Mesoscale Processes,* Portland, OR, Amer. Meteor. Soc., 151–153.

Bacmeister, J. T., P. J. Pegion, S. D. Schubert, and M. J. Suarez, 2000: Atlas of seasonal means simulated by the NSIPP 1 atmospheric GCM. NASA/TM-2000-104505, Vol. 17, 194 pp.

Bell, T. L., and N. Reid, 1993: Detection of the diurnal cycle of tropical rainfall from satellite observations. *J. Appl. Meteor.,* **32,** 311–322.

Betts, A., J. H. Ball, A. C. M. Beljaars, M. J. Miller, and P. A. Viterbo, 1996: The land surface–atmosphere interaction: A review based on observational and global modeling perspectives. *J. Geophys. Res.,* **101,** 7209–7225.

Carbone, R. E., J. D. Tuttle, D. A. Ahijevych, and S. B. Trier, 2002: Inferences of predictability associated with warm season precipitation episodes. *J. Atmos. Sci.,* **59,** 2033–2056.

Chen, M., R. E. Dickinson, X. Zeng, and A. N. Hahmann, 1996: Comparison of precipitation observed over the continental United States to that simulated by a climate model. *J. Climate,* **9,** 2233–2249.

Collier, J. C., and K. P. Bowman, 2004: Diurnal cycle of tropical precipitation in a general circulation model. *J. Geophys. Res.,* **109,** D17105, doi:10.1029/2004JD004818.

Dai, A., 2001: Global precipitation and thunderstorm frequencies. Part II: Diurnal variations. *J. Climate,* **14,** 1112–1128.

——, 2006: Precipitation characteristics in eighteen coupled climate models. *J. Climate,* **19,** 4605–4630.

——, and C. Deser, 1999: Diurnal and semidiurnal variations in global surface wind and divergence fields. *J. Geophys. Res.,* **104,** 31 109–31 125.

——, and K. E. Trenberth, 2004: The diurnal cycle and its depiction in the Community Climate System Model. *J. Climate,* **17,** 930–951.

——, F. Giorgi, and K. E. Trenberth, 1999: Observed and model-simulated diurnal cycles of precipitation over the contiguous United States. *J. Geophys. Res.,* **104,** 6377–6402.

Figueroa, S. N., P. Satyamurty, and P. L. Silva Dias, 1995: Simulations of the summer circulation over the South American region with an eta coordinate model. *J. Atmos. Sci.,* **52,** 1573–1584.

Gandu, A. W., and P. L. Silva Dias, 1998: Impact of tropical heat sources on the South American tropospheric upper circulation and subsidence. *J. Geophys. Res.,* **103,** 6001–6015.

Garratt, J. R., P. B. Krummel, and E. A. Kowalczyk, 1993: The surface-energy balance at local and regional scales—A comparison of general circulation model results with observations. *J. Climate,* **6,** 1090–1109.

Gill, A. E., 1980: Some simple solutions for heat induced tropical circulation. *Quart. J. Roy. Meteor. Soc.,* **106,** 447–462.

Giorgi, F., and C. Shields, 1999: Tests of precipitation parameterizations available in latest version of NCAR Regional Climate Model (RegCM) over continental United States. *J. Geophys. Res.,* **104,** 6353–6376.

Gochis, D. G., A. Jimenez, C. J. Watts, J. Garatuza-Payan, and W. J. Shuttleworth, 2004: Analysis of 2002 and 2003 warm-season precipitation from the North American Monsoon Experiment event rain gauge network. *Mon. Wea. Rev.,* **132,** 2938–2953.

Groisman, P. Ya., R. S. Bradley, and B. Sun, 2000: The relationship of cloud cover to near-surface temperature and humidity: Comparison of GCM simulations with empirical data. *J. Climate,* **13,** 1858–1878.

Helfand, H. M., and S. D. Schubert, 1995: Climatology of the simulated Great Plains low-level jet and its contribution to the continental moisture budget of the United States. *J. Climate,* **8,** 784–806.

Higgins, R. W., J. E. Janowiak, and Y. Yao, 1996: A gridded hourly precipitation data base for the United States (1963–1993). NCEP/Climate Prediction Center Atlas 1, 47 pp.

——, Y. Yao, E. S. Yarosh, J. E. Janowiak, and K. C. Mo, 1997: Influence of the Great Plains low-level jet on the summertime precipitation and moisture transport over the central United States. *J. Climate,* **10,** 481–507.

——, W. Shi, E. Yarosh, and R. Joyce, 2000: Improved United States precipitation quality control system and analysis. NCEP/Climate Prediction Center Atlas 7, 40 pp.

Higgins, W., and Coauthors, 2006: North American Monsoon Experiment (NAME) 2004 field campaign and modeling strategy. *Bull. Amer. Meteor. Soc.,* **87,** 79–94.

Janowiak, J. E., V. J. Dagostaro, V. E. Kousky, and R. J. Joyce, 2007: An examination of precipitation in observations and model forecasts during NAME with emphasis on the diurnal cycle. *J. Climate,* **20,** 1680–1692.

Joyce, R. J., J. E. Janowiak, P. A. Arkin, and P. Xie, 2004: CMORPH: A method that produces global precipitation estimates from passive microwave and infrared data at high spatial and temporal resolution. *J. Hydrometeor.,* **5,** 487–503.

Koster, R. D., and Coauthors, 2004: Regions of strong coupling between soil moisture and precipitation. *Science,* **305,** 138–1140.

Lee, M.-I., and Coauthors, 2007: An analysis of the warm-season diurnal cycle over the continental United States and northern Mexico in general circulation models. *J. Hydrometeor.,* in press.

Liang, X.-Z., L. Li, A. Dai, and K. E. Kunkel, 2004: Regional climate model simulation of summer precipitation diurnal cycle over the United States. *Geophys. Res. Lett.,* **31,** L24208, doi:10.1029/2004GL021054.

Lim, G. H., and A. S. Suh, 2000: Diurnal and semidiurnal variations in the time series of 3-hourly assimilated precipitation by NASA GEOS-1. *J. Climate,* **13,** 2923–2940.

Lin, X., D. A. Randall, and L. D. Fowler, 2000: Diurnal variability of the hydrological cycle and radiative fluxes: Comparisons between observations and a GCM. *J. Climate,* **13,** 4159–4179.

Machado, L. A. T., H. Laurent, and A. A. Lima, 2002: The diurnal march of the convection observed during TRMM-WETAMC/LBA. *J. Geophys. Res.,* **107,** 8064, doi:10.1029/2001JD000338.

——, ——, N. Dessay, and I. Miranda, 2004: Seasonal and diurnal variability of convection over the Amazonia: A comparison of different vegetation types and large scale forcing. *Theor. Appl. Climatol.,* **78,** 61–77.

Maddox, R. A., 1980: Mesoscale convective complexes. *Bull. Amer. Meteor. Soc.,* **61,** 1374–1387.

Mesinger, F., and Coauthors, 2006: North American Regional Reanalysis. *Bull. Amer. Meteor. Soc.,* **87,** 343–360.

Randall, D. A., Harshvardhan, and D. A. Dazlich, 1991: Diurnal variability of the hydrological cycle in a general circulation model. *J. Atmos. Sci.,* **48,** 40–62.

Rasmusson, E. M., 1967: Atmospheric water vapor transport and the water balance of North America: Part I. Characteristics of the water vapor flux field. *Mon. Wea. Rev.,* **95,** 403–426.

Reynolds, R. W., N. A. Rayner, T. M. Smith, D. C. Stokes, and W. Wang, 2002: An improved in situ and satellite SST analysis for climate. *J. Climate,* **15,** 1609–1625.

Riley, G. T., M. G. Landin, and L. F. Bosart, 1987: The diurnal variability of precipitation across the central Rockies and adjacent Great Plains. *Mon. Wea. Rev.,* **115,** 1161–1172.

Schubert, S. D., H. M. Helfand, C.-Y. Wu, and W. Min, 1998: Subseasonal variations in warm-season moisture transport and precipitation over the central and eastern United States. *J. Climate,* **11,** 2530–2555.

Silva Dias, P. L., J. P. Bonatti, and V. E. Kousky, 1987: Diurnally forced tropical tropospheric circulation over South America. *Mon. Wea. Rev.,* **115,** 1465–1478.

Slingo, A., R. C. Wilderspin, and S. J. Brentnall, 1987: Simulation of the diurnal cycle of outgoing longwave radiation with an atmospheric GCM. *Mon. Wea. Rev.,* **115,** 1451–1457.

Tian, B., I. M. Held, N.-C. Lau, and B. J. Soden, 2005: Diurnal cycle of summertime deep convection over North America: A satellite perspective. *J. Geophys. Res.,* **110,** D08108, doi:10.1029/2004JD005275.

Wallace, J. M., 1975: Diurnal variations in precipitation and thunderstorm frequency over the conterminous United States. *Mon. Wea. Rev.,* **103,** 406–419.

Yang, G. Y., and J. Slingo, 2001: The diurnal cycle in the Tropics. *Mon. Wea. Rev.,* **129,** 784–801.

Zhang, G. J., 2003: Roles of tropospheric and boundary layer forcing in the diurnal cycle of convection in the U.S. southern Great Plains. *Geophys. Res. Lett.,* **30,** 2281, doi:10.1029/2003GL018554.